Final published version of this article: Journal of Physics and Chemistry of Solids, Volume 179, August 2023, 111426
Available online: 6 May 2023
DOI: https://doi.org/10.1016/j.jpcs.2023.111426

Charge transfer in $Nb_{1-x}V_xSe_2$ materials: synchrotron radiation spectroscopy study

A.I. Merentsov[1], A.S. Shkvarin[1,2], E.M. Sherokalova[3], I. Píš[4,5], F. Bondino[5], A.N. Titov[1]

[1] M.N. Miheev Institute of Metal Physics of Ural Branch of Russian Academy of Sciences, 620990 Ekaterinburg, Russia

[2] Ural State Mining University, 620144 Ekaterinburg, Russia

[3] Ural Federal University, 620002 Ekaterinburg, Russia

[4] Elettra-Sincrotrone Trieste S.C.p.A, S.S. 14 – km 163.5, 34149 Basovizza, Trieste, Italy

[5] IOM-CNR, Istituto Officina dei Materiali, S.S. 14 – km 163.5, 34149 Basovizza, Trieste, Italy

The electronic structure of the single-crystalline solid solutions $Nb_{1-x}V_xSe_2$ has been studied using soft X-ray photoelectron, resonant photoelectron, and absorption spectroscopy. A charge transfer between VSe_2 and $NbSe_2$ sublattices was observed. This charge transfer makes the octahedral coordination of the Nb atoms by Se atoms preferable as compared to the trigonal-prismatic coordination in undoped $NbSe_2$.

Introduction

Layered transition metal dichalcogenides (LTMDs) with a general formula MCh_2 (with M – 3d- or 4d-transition metal; Ch = S, Se, Te) have attracted scientific interest over the last few decades [1–5] for both their fundamental [6–8] and applied [9–12] properties. $NbSe_2$ is a member of a wide LTMDs family and is particularly attractive for its superconductivity [13,14] and charge-density-wave state [15,16]. $NbSe_2$ is also used as an anode material for Li-ion batteries [17,18] and the host lattice for hydrogen intercalation [19–21]. Similarly, VSe_2 can also be used as an anode material for Li-ion batteries [22,23]. A charge-density-wave state transition occurs in VSe_2 at a much higher temperature (~ 100 K) [24–26] than that in $NbSe_2$ (~ 30 K) [27]. The similarity of the electronic and electrochemical properties of these two materials originates from the same configuration of the external electron orbitals; both Nb^{4+} and V^{4+} give one electron into the MSe_2 (M = Nb, V) conduction band. This similarity suggests the possibility of mutual substitution of the Nb and V atoms in the $Nb_{1-x}V_xSe_2$ lattice without substantial distortions. At the same time, it was shown that such substitution in the nd-transition metal sublattice provides in some cases an improvement of the electrochemical properties of LTMDs [28]. For example, $Mo_{0.5}Nb_{0.5}Se_2$ exhibits much higher electrocatalytic performance for hydrogen evolution reaction compared to $MoSe_2$ and $NbSe_2$ [29].

The crystal structure of polycrystalline $Nb_{1-x}V_xSe_2$ with x = 0 – 1 has been studied previously [30]. According to these results, there are three regions of homogeneity in the $Nb_{1-x}V_xSe_2$ materials corresponding to 2H ($0 \le x < 0.01$), 4Hb ($0.11 \le x \le 0.2$) and 1T ($0.3 \le x \le 1.0$) polytypes. In the 2H polytype both the Nb and V atoms are in the trigonal-prismatic environment coordinated by six Se atoms, the 4Hb polytype contains the Nb atoms in the trigonal-prismatic coordination and V atoms in octahedral coordination, and the 1T polytype is characterized by only octahedral coordination for both the V and Nb atoms. The study of the magnetic and electric properties of polycrystalline 2H-$Nb_{1-x}V_xSe_2$ with $x \le 0.1$ showed the suppression of the superconducting transition typical for $NbSe_2$ [31].

The current work reports on the electronic structure study of $Nb_{1-x}V_xSe_2$ single-crystal samples in dependence on the local environment of Nb and V atoms coordinated by Se. We have

chosen two chemical compositions of the $Nb_{1-x}V_xSe_2$ compounds with x = 0.1 and x = 0.6 corresponding to the different coordination of the Nb and V atoms. In $Nb_{0.9}V_{0.1}Se_2$ the Nb atoms are in the trigonal-prismatic environment of the Se atoms, while in $Nb_{0.4}V_{0.6}Se_2$ they are in the octahedral environment of the Se atoms. At the same time, in both compounds the V atoms do not change their octahedral environment of the Se atoms. The electronic structure has been investigated using a combination of X-ray photoelectron spectroscopy (XPS), resonant X-ray photoelectron spectroscopy (ResPES), and X-ray absorption spectroscopy (XAS).

Experimental

Polycrystalline $Nb_{1-x}V_xSe_2$ materials with x = 0.1 and x = 0.6 were prepared using the high-temperature solid state reaction method. Niobium (99.98%), vanadium (99.95%), and selenium (OSCh19-5, 99.999%) were used as starting materials. The materials were synthesized in sealed quartz ampoules evacuated to 10^{-5} Torr at a temperature of 900 ^{o}C for 1 week with a minimal temperature gradient. The single crystals were grown during the synthesis of the polycrystalline material in the same ampoule. The planar size of the crystals grown was approximately 5 × 5 mm^2 with a thickness of about 10 μm. The chemical composition of the single crystals was determined using energy dispersive X-ray analysis (EDAX) with a Quanta 200 Pegasus spectrometer in the Collective Use Center 'Testing Center for Nanotechnology and Prospective Materials' of the Institute of Metal Physics, Russian Academy of Sciences, Ural Division.

The X-ray diffraction (XRD) study of the $Nb_{1-x}V_xSe_2$ powders and single crystals was performed using a Bruker AXS D8 Advance diffractometer (room temperature, Cu $K\alpha_{1,2}$ radiation, Göbel mirror monochromator, and a set of Soller slits for limiting the axial divergence of the diffracted beam).

The synchrotron radiation XPS, XAS and ResPES spectra of $Nb_{1-x}V_xSe_2$ were obtained at the IOM CNR BACH beamline [32] at the Elettra synchrotron facility (Trieste, Italy). The experiments were performed on $Nb_{1-x}V_xSe_2$ single crystals cleaved in situ in an ultra-high vacuum chamber at a pressure lower than 1×10^{-9} Torr. The purity of the samples' surface was confirmed by the absence of oxygen and carbon peaks in the survey spectra. Incident synchrotron radiation was polarized linearly with the polarization vector lying in the scattering plane. The XPS and ResPES spectra were measured at normal emission with a Scienta R3000 electron energy analyzer at an angle of 60° from the incident beam direction and the total energy resolution was 0.2 eV. Binding energies were calibrated to the Fermi edge measured on a clean Au foil in electrical contact with the samples. The photon energies were calibrated using the difference in the kinetic energy of Au 4f line recorded in the first- and second-order light. Nb $M_{2,3}$ and V $L_{2,3}$ XAS were performed in total electron yield by measuring the drain current through the sample. Photon energy resolution was set to 0.1 eV. All measurements were performed at room temperature. The XPS peak fitting was performed using KolXPD software [33].

Results

Crystal structure

Since we used the XRD method only for testing the quality of the grown single crystals, the diffraction patterns are not able to give full information about the crystal structure of the studied materials. Therefore, the XRD patterns are given in Supporting Information file (Fig. S1)

and are not included in the main text of this work. The narrow intense peaks indicate a good quality of the single crystals and their homogeneity. While the diffraction patterns were obtained on a powder single-axis diffractometer, we can observe only the diffraction peaks derived from the (00l) planes. This is also the reason why we cannot make an unambiguous choice between the 2H, 4Hb or 1T polytypes to describe the crystal structure of the studied single crystals. Taking the 1T model ($P\bar{3}m1$ space group) for $Nb_{0.4}V_{0.6}Se_2$ and 2H one ($P6_3/mmc$ space group) for $Nb_{0.9}V_{0.1}Se_2$ (as proposed in Ref. [30]), we calculated the lattice parameter c_0 for both single crystals. For $Nb_{0.4}V_{0.6}Se_2$ c_0 = 6.155 Å, for $Nb_{0.9}V_{0.1}Se_2$ c_0 = 6.195 Å. These values are in good agreement with those obtained for the initial powder samples (see Figure S2) and with those reported in Ref. [30]. The XRD measurements do not permit obtaining both values of the a lattice parameter and atomic coordinates, however, they provide information about the overall quality of the studied crystals.

Chemical composition and morphology

Figure 1 shows scanning electron microscopy (SEM) images of single crystals of two compositions we synthesized. The rectangles indicate the areas used to measure the X-ray spectra for EDAX chemical analysis. The first crystal (Fig 1a), grown from the $Nb_{0.9}V_{0.1}Se_2$ charge, has the exact composition of $Nb_{0.87}V_{0.095}Se_2$. The second crystal (Fig. 1b), grown from the $Nb_{0.4}V_{0.6}Se_2$ charge, has the composition of $Nb_{0.37}V_{0.63}Se_2$. As we can see, the chemical composition of the single crystals is very close to the stoichiometry of the initial charge. Therefore, we will refer to these crystals by the composition of the corresponding charge. The chemical composition of the $Nb_{0.4}V_{0.6}Se_2$ crystal was additionally confirmed by the XPS data and is consistent with the chemical composition of the powder sample. The morphology of the crystals is similar; we can clearly see light-grey and dark-grey areas, however, we cannot distinguish their chemical composition based on EDAX data, which give us an averaged composition of the areas. A possible explanation for this morphology is proposed in the Discussion section.

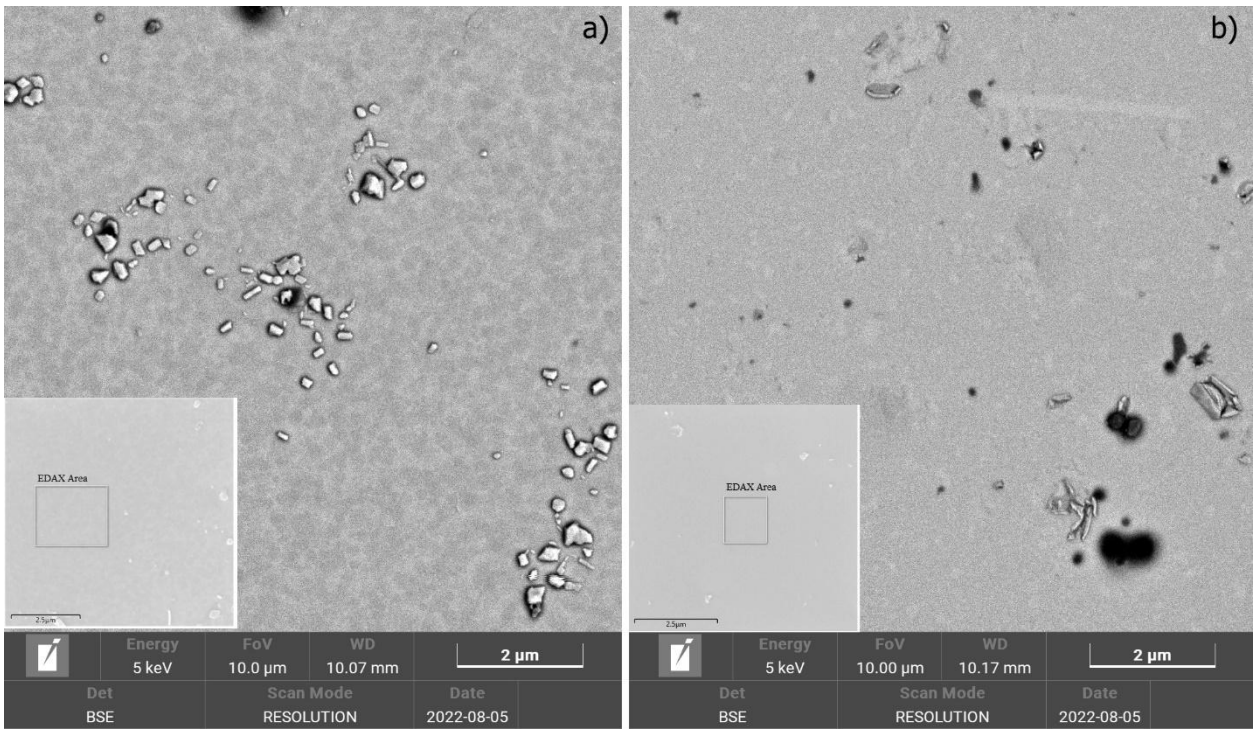

Figure 1. SEM images of the $Nb_{0.9}V_{0.1}Se_2$ (a) and $Nb_{0.4}V_{0.6}Se_2$ (b) single crystals. The insets show the scale of the EDAX spectra measurements.

Core-level XPS

The core level spectra provide information about both the charge state of the atoms and the quality of the sample surface. Figure S3 shows the survey spectra for the $NbSe_2$, $Nb_{0.9}V_{0.1}Se_2$, $Nb_{0.4}V_{0.6}Se_2$ and VSe_2 single crystals. The absence of C 1s and O 1s peaks indicates good quality of the crystal surface. The absence of the O 1s peak also exclude oxide impurities in the sample. The Se 3d core level spectrum is a good indicator of any heterogeneity or phase mixture in the material [34,35]. Figure 2 shows the Se 3d spectra for the studied $Nb_{1-x}V_xSe_2$ materials.

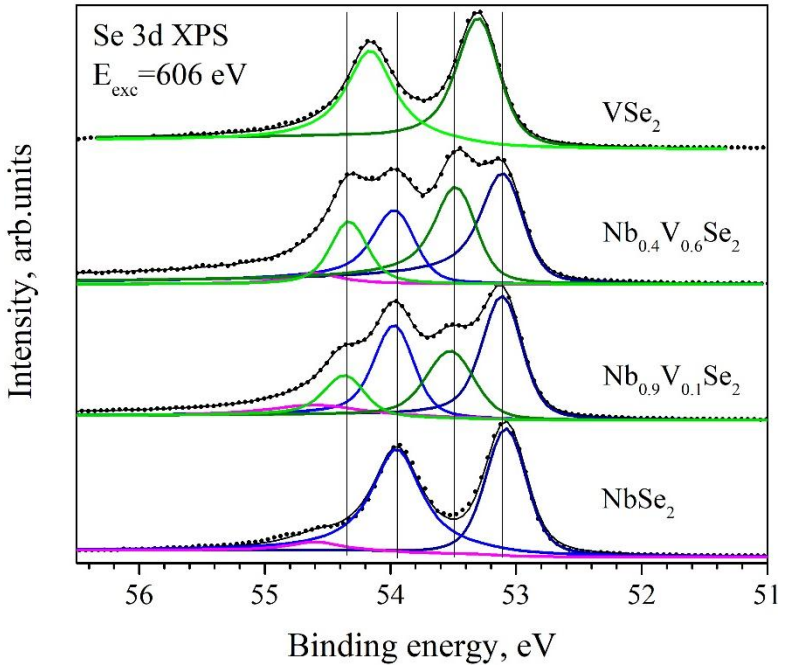

Figure 2. Se 3d core-level spectra for $Nb_{1-x}V_xSe_2$. The blue 3d doublet corresponds to the Se 3d states in $NbSe_2$, the green one corresponds to the Se 3d states in VSe_2.

The substitution of Nb by V atoms results in the additive Se 3d spectrum. This means that the Se 3d spectrum for both $Nb_{0.9}V_{0.1}Se_2$ and $Nb_{0.4}V_{0.6}Se_2$ is composed of Se 3d doublets with binding energies typical for VSe_2 ($E_b(Se\ 3d_{5/2})$ = 53.3 eV) and $NbSe_2$ $E_b(Se\ 3d_{5/2})$ = 53.1 eV. The Se 3d binding energy in the $NbSe_2$ sublattice (blue lines in Fig. 2) is lower than that in the VSe_2 sublattice (green lines in Fig. 2), and it remains constant during the Nb by V substitution. At the same time, the Se 3d binding energy in the VSe_2 sublattice increases ($E_b(Se\ 3d_{5/2})$ = 53.5 eV) compared to undoped VSe_2 and does not depend on the V concentration.

Figure 3 shows the Nb 3d core level spectra for $Nb_{1-x}V_xSe_2$ and a well-resolved Nb 3d spectrum for undoped $NbSe_2$. Its structure with a main line ($E_b(Nb\ 3d_{3/2})$ = 203 eV, orange curve) and a high-binding energy shoulder ($E_b(Nb\ 3d_{3/2})$ = 203.5 eV, red line in Fig. 3) is consistent with the data previously reported for $NbSe_2$ [36]. The shoulder has been assigned to the crystal field multiplet splitting [37,38]. A contribution from Nb^{4+} or Nb^{5+} can be excluded because no oxygen was detected by XPS (Fig. S3). A change in the multiplet is caused by the change in the local environment of the Nb atoms. Namely, we can consider the change in the

intensity of the ionic interaction between the Nb atom and nearest Se atoms. Comparing our Nb 3d XPS spectra with that from Ref. [38] for NbO_2, we find that the best coincidence in shape is for $Nb_{0.4}V_{0.6}Se_2$. This is due to the higher ionicity of oxygen as compared to selenium, which implies "higher" charge transfer from Nb to O as compared to that from Nb to Se. Therefore, we can attribute the change in the shape of the Nb 3d XPS to the charge transfer from the Nb atoms.

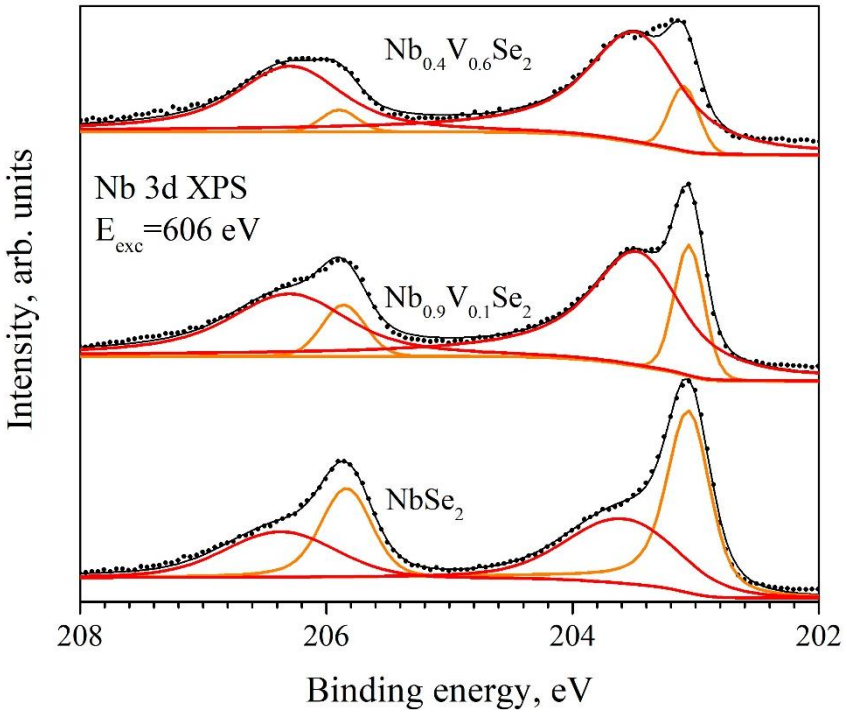

Figure 3. Nb 3d core-level spectra for $Nb_{1-x}V_xSe_2$.

Nb $M_{2,3}$ XAS (Fig. S4 (b)) is consistent with the Nb 3d core level spectra and substantially broadens for $Nb_{0.4}V_{0.6}Se_2$ as compared to $NbSe_2$, which is due the change in the local coordination of the Nb atoms by Se ones.

Valence band XPS

The valence band (VB) spectra for $Nb_{1-x}V_xSe_2$ shown in Fig. 4 are typical for transition metal dichalcogenides. Several bands (marked as L, T, Q, M, R) can be distinguished in the spectra. The Se 4s band has a binding energy of 13.2 eV. This band is slightly broader for $Nb_{1-x}V_xSe_2$ solid-solution compared with the Se 4s for the reference $NbSe_2$ and VSe_2 crystals, similarly as it was observed in the Se 3d spectra. All the spectra contain the L band, while the M band is a feature of only the Nb-containing crystals and the Q band is a feature of only the V-containing crystals. As we can see, the Q band is 0.35 eV shifted toward higher binding energies for the $Nb_{1-x}V_xSe_2$ compounds compared to VSe_2. The T band is present in all the spectra, however, its binding energy is different in $NbSe_2$ and VSe_2 crystals. In the $Nb_{0.9}V_{0.1}Se_2$ and $Nb_{0.4}V_{0.6}Se_2$ crystals, the binding energy of the T band is E_b = 3.4 eV, 0.4 eV higher than that in VSe_2. This difference in the binding energies can be explained by the formation of new states near the Fermi level in the $Nb_{1-x}V_xSe_2$ compounds as compared to undoped VSe_2 and $NbSe_2$. Finally, a narrow R band is well visible near the Fermi level for all compounds. To separate the V and Nb contributions to this band, resonant X-ray photoelectron spectra were acquired.

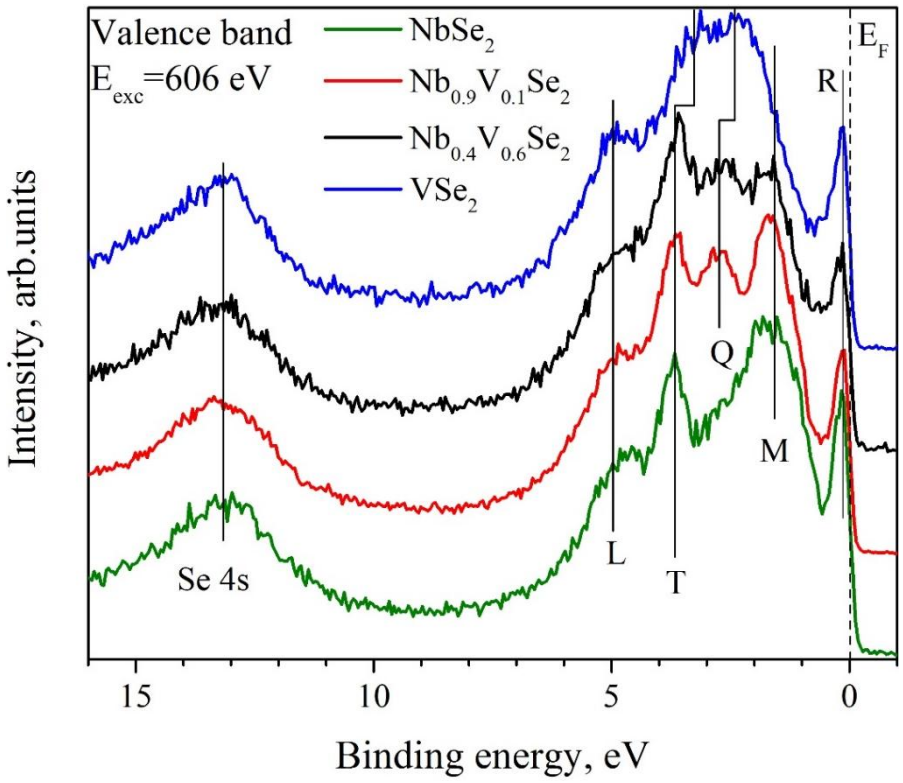

Figure 4. Valence band (VB) spectra for $Nb_{1-x}V_xSe_2$.

Resonant photoelectron spectroscopy provides element-specific information on the energy localization of the electronic states. Selecting the incident photon energy slightly larger than the binding energy of the selected core level upon excitation of the np electrons (n = 2; 3; 4) to an unfilled nd state enhances the photoemission of d electrons from nd metals and their compounds. This results in a resonant electron emission [39–42]. The energy of the resonance maximum corresponds to the transition from resonant Raman-Auger spectra (RRAS) to normal Auger spectra [43]. Resonant photoelectron spectroscopy is a good “detector” for the charge transfer into the vacant states of the valence band. We can detect the hybrid states appeared near the Fermi level on the valence band spectra obtained across the core level-valence band resonance excitation.

Figure 5 shows the VB spectra obtained across the V 2p-3d resonant excitation. The intensity of the resonant peak at the Fermi level decreases with V concentration. The on-maximum spectra obtained across the V 2p-3d resonant excitation (Fig. 6) clearly indicate a 1.5-fold decrease in the intensity of the resonant peak taking the intensity of the RRAS peak as 1.

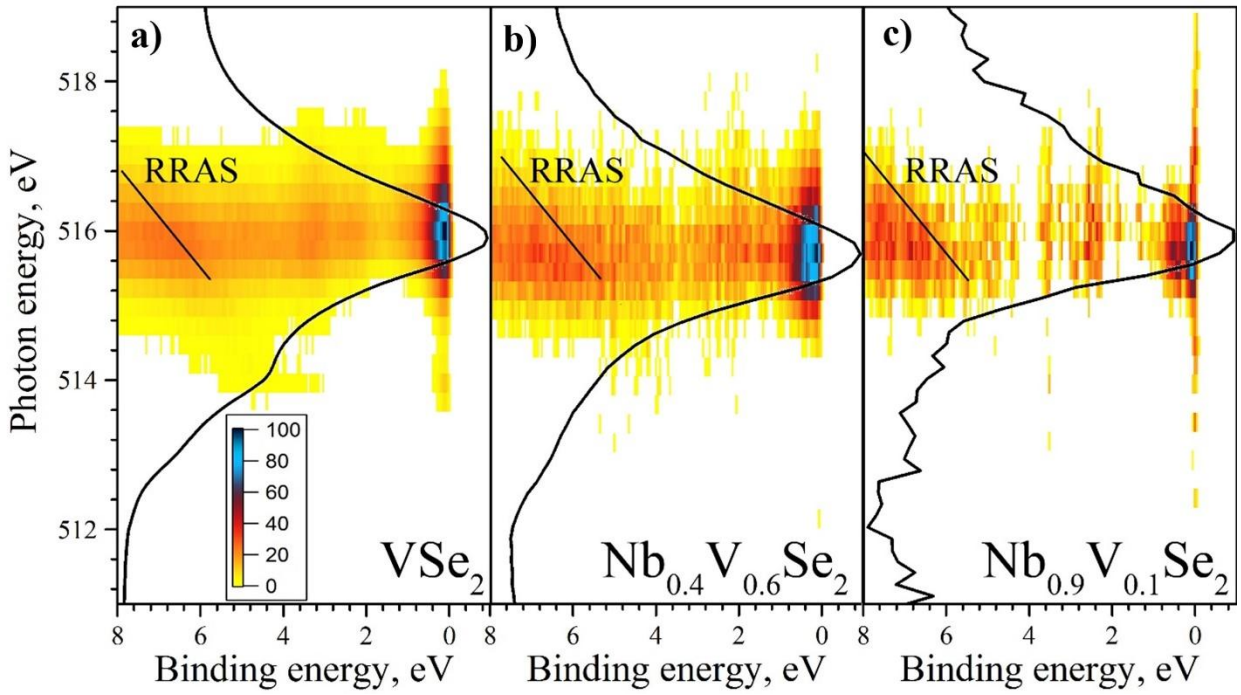

Figure 5. VB spectra for $Nb_{1-x}V_xSe_2$ with x = 1 (a), x = 0.6 (b) and x = 0.1 (c), obtained across the V 2p-3d resonance excitation.

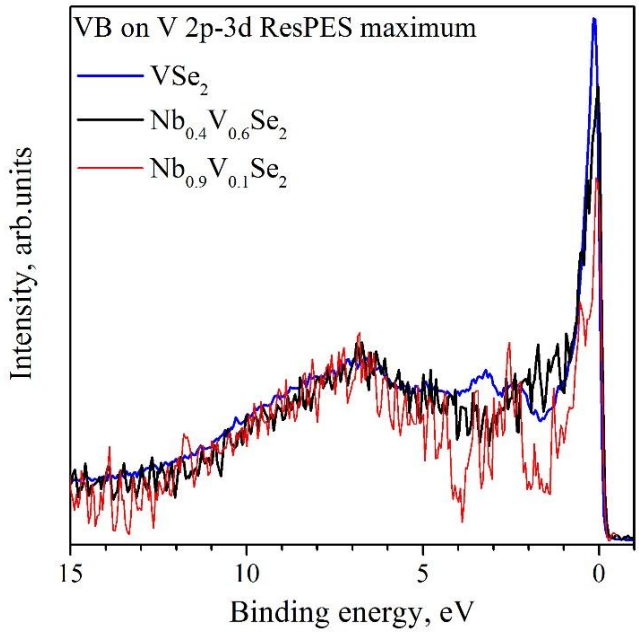

Figure 6. Valence band spectra for $Nb_{1-x}V_xSe_2$ obtained with photon energies corresponding to maximum resonant enhancement across the V 2p-3d excitation.

Our previous results on the $V_{1-x}Ti_xSe_2$ system [44] clearly showed the independence of the intensity ratio of the resonant and RRAS peaks both on the Ti and V concentration. In contrast to the $V_{1-x}Ti_xSe_2$ system, where a charge transfer from VSe_2 to $TiSe_2$ lattice was minimal, here obtained ResPES spectra indicate that a charge transfer occurs in the $Nb_{1-x}V_xSe_2$ system.

Figure 7 shows the VB spectra obtained across the Nb 3p-4d resonant excitation. Although the resonance is weak in all cases, some significant differences can be found. No resonance is observed for $NbSe_2$ (Fig. 7 a) near the Fermi level. On the other hand, even a small

amount of the V atoms substituting Nb atoms results in the appearance of the resonant peak just above the Fermi level (highlighted with a red oval in Fig. 7b). The intensity of this resonant peak remains almost constant as the V concentration increases, however other features at the binding energies of E_b = 4 eV and E_b = 7 eV noticeably disappear (Fig. 7c).

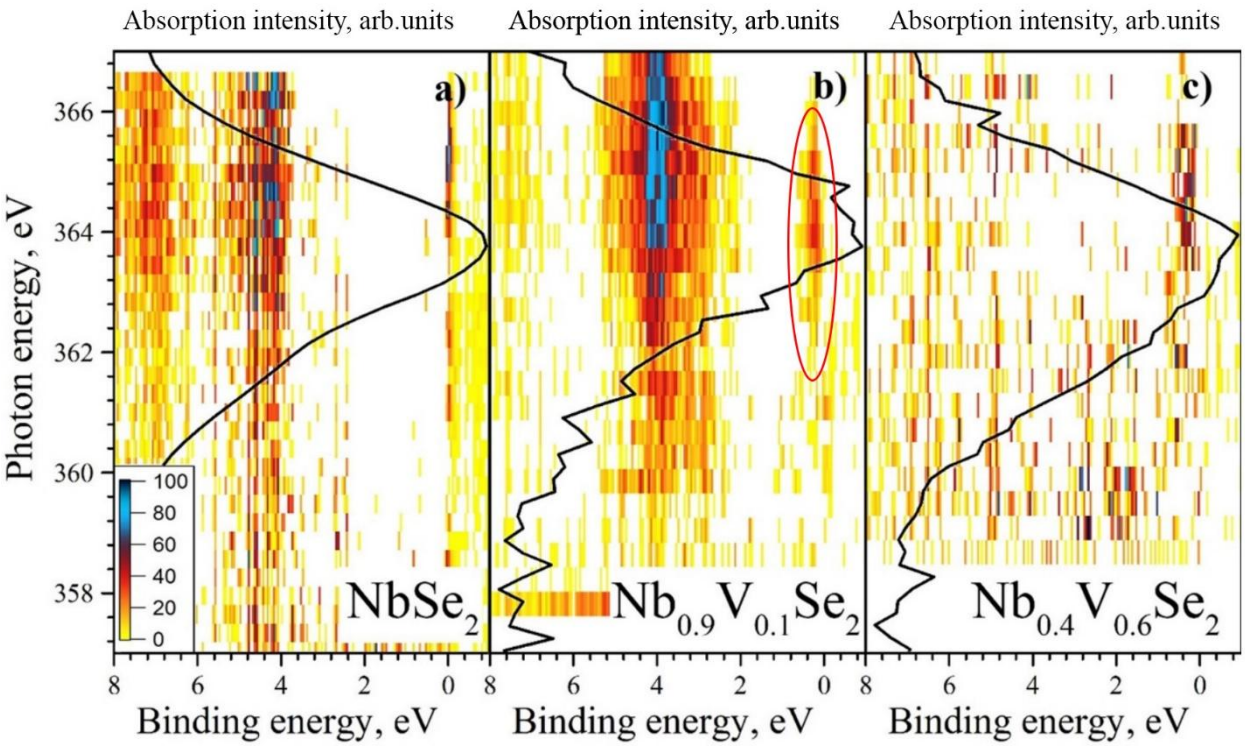

Figure 7. The VB spectra for $Nb_{1-x}V_xSe_2$ with x = 0 (a), x = 0.1 (b) and x = 0.6 (c), obtained across the Nb 3p-4d resonance excitation. Solid curves are XAS spectra measured in total electron yield mode simultaneously with the ResPES maps.

Discussion

The obtained experimental data, in particular the binding energy shift of the Se 3d states, decrease of the intensity of the resonant band at the V 2p-3d resonant excitation, and changes in the VB spectra, suggest that there is a charge transfer between the $NbSe_2$ and VSe_2 sublattices. However, determining the direction of this transfer might not be straightforward. The observed increase in the binding energy of the Se 3d states in the VSe_2 sublattice can be due to i) the charge transfer from the V to Nb atoms in the homogeneous solid solution (all the atoms of the transition metals are uniformly mixed within the atomic layer) or ii) the charge transfer from the $NbSe_2$ to VSe_2 sublattices in the inhomogeneous solid solution (the distribution of the transition metal atoms is not uniform, there are areas of prevailing $NbSe_2$ or VSe_2 sublattices). In the first case, the Se atoms coordinating the V atoms can decrease their negative charge and, therefore, increase the binding energy. The second case means the increase in the Fermi energy in the VSe_2 sublattice, which could be visible on the V 2p core level shift in the same direction as the Se 3d core level. However, low intensity of the V 2p signal (see Fig. S5) do not allow us to make an unambiguous conclusion about it. The shift of the Fermi energy could be also visible in the Se 3d and Nb 3d core-level spectra for the $NbSe_2$ sublattice. However, the Se 3d and Nb 3d binding energies in the $NbSe_2$ sublattice do not change significantly at the Nb by V substitution while the trigonal-prismatic coordination of the Nb atoms by the Se ones in $NbSe_2$ and $Nb_{0.9}V_{0.1}Se_2$ changes to octahedral one in $Nb_{0.4}V_{0.6}Se_2$. The change in the Nb 3d and Se 3d charge states due to the change in the coordination of the Nb atoms by Se ones can be

compensated by the Fermi energy shift due to the charge transfer from the $NbSe_2$ to VSe_2 sublattice. The shift of the Fermi energy would correspond to the case of the formation of the VSe_2 and $NbSe_2$ structural units. It's worth to note that these units are not the separated phases of VSe_2 and $NbSe_2$ but thin (~30Å) and small (less than 100 μm) electrically charged areas of the single crystal differing in the local chemical composition. A strong indication supporting this mechanism is the additive structure of the $Nb_{1-x}V_xSe_2$ Se 3d doublets, which are similar to those previously observed for the single crystals in the $Cr_xTi_{1-x}Se_2$ system. The existence of the $CrSe_2$-based and $TiSe_2$-based structural units in the $Cr_xTi_{1-x}Se_2$ materials was confirmed by the X-ray scanning photoemission microscopy (SPEM) measurements [45]. In the case of the homogeneous solid solution, one should expect a monotonic change in the Se 3d binding energies without the additive structure of the spectrum. On the other hand, in the case of the inhomogeneous solid solution, the volume fraction of the VSe_2 and $NbSe_2$ units should match the contributions of the Se 3d doublets from the VSe_2 and $NbSe_2$ sublattices to the total Se 3d spectrum. For the $Nb_{0.4}V_{0.6}Se_2$ crystal, $I_{Se3d}(NbSe_2)/I_{Se3d} = 0.38$, where I is the integral intensity of the peak, I_{Se3d} is the total integral intensity of the Se 3d spectrum. This means that the $Nb_{0.4}V_{0.6}Se_2$ crystal can be described as $0.38 \cdot NbSe_2 + 0.62 \cdot VSe_2$. For the $Nb_{0.9}V_{0.1}Se_2$ crystal, $I_{Se3d}(NbSe_2)/I_{Se3d} = 0.60$, which result in the composition $0.60 \cdot NbSe_2 + 0.40 \cdot VSe_2$. For this crystal, there is a rather large discrepancy between the $NbSe_2$ and VSe_2 volume fractions and the chemical composition. This overestimation of the VSe_2 contribution can be due to the peculiarity of the cleaving procedure of the crystal before the experiment; since the crystals of the LTMDs split in the regions with weakest bonding, it seems that there should be more units on the surface, that are relatively weaker bonded with each other (1T-VSe_2) than those that are stronger bonded (2H-$NbSe_2$). The light-grey and dark-grey areas observed on the SEM images may correspond to these VSe_2- and $NbSe_2$-based units.

For all the studied compounds the V atoms are in the octahedral coordination by the Se atoms. At the same time, the Nb atoms change their trigonal-prismatic ("T-P") coordination by the Se atoms in $NbSe_2$ and $Nb_{0.9}V_{0.1}Se_2$ to the octahedral ("O") one in $Nb_{0.4}V_{0.6}Se_2$. According to the band scheme of the LTMDs proposed by Wilson and Yoffe [1] and confirmed by numerous studies (e.g. [46–48]), the main difference between the LTMDs with the "T-P" and "O" coordination of the TM atoms consists in the energy of the d_z^2 band forming the bottom of the conduction band; the binding energy of the d_z^2 band is higher for the "T-P" coordination than for the "O" one. Therefore, the "T-P"-to-"O" crossover of the Nb atoms must be accompanied by the charge transfer from $NbSe_2$ to VSe_2. Since the Nb 4d ionization energy (I_2 = 14.3 eV) is lower than the V 3d ionization energy (I_3 = 29.3 eV), one should expect that the "T-P"-to-"O" crossover of the Nb atoms must lead to the increased filling of the V 3d-derived band in $Nb_{0.4}V_{0.6}Se_2$ as compared even to VSe_2, where all the V atoms are in the "O" coordination. Such a filling of the valence band decreases the density of empty states and, therefore, leads to the decrease of the intensity of the resonant band in the ResPES experiment. The results obtained, namely an increase in the Se 3d binding energy for the VSe_2 subsystem, a change of the Nb 3d spectrum at the "T-P"-to-"O" crossover and a decrease of the intensity of the resonant band across the V 2p-3d resonant excitation, are fully in line with these expectations.

Conclusions

The synchrotron radiation spectroscopy study of the $Nb_{1-x}V_xSe_2$ materials allowed the direct observation of the charge transfer between the $NbSe_2$ and VSe_2 sublattices. Despite the XPS method is not a direct one, such as, for example, X-ray scanning photoemission microscopy

(SPEM), and does not allow direct observation of inhomogeneities in single crystals, the Se 3d spectrum has the same additive structure, as we previously observed for the $Cr_xTi_{1-x}Se_2$ single crystals. As the morphology of the $Cr_xTi_{1-x}Se_2$ single crystals was confirmed to consist of the $CrSe_2$- and $TiSe_2$-based structural units, we believe that the morphology of the $Nb_{1-x}V_xSe_2$ single crystals is the same and consists of the VSe_2- and $NbSe_2$-based structural units. Based on the observed energy shift of the Se 3d core-level spectrum, change of the Nb 3d spectrum, and decrease in the intensity of the resonant band across the V 2p-3d resonant excitation, we can assume that the direction of the charge transfer is from $NbSe_2$ to VSe_2. This transfer makes the octahedral coordination of Nb atoms by Se ones preferable as compared to trigonal-prismatic coordination. At the same time, V atoms do not change their coordination at this charge transfer.

Thus, control of the coordination of transition metal atoms by the chalcogen atoms in LTMDs-based solid solutions can act as a tool for redistribution of electrons between either TM atoms or the $TMCh_2$ (Ch = S, Se, Te) structural units, depending on the morphology of the studied materials.

Supporting Information

See the supporting information for X-ray diffraction characterization of the $Nb_{0.9}V_{0.1}Se_2$ and $Nb_{0.4}V_{0.6}Se_2$ powders and single crystals, survey XPS spectra, V $L_{2,3}$ and Nb $L_{2,3}$ X-ray absorption spectra, V 2p core-level XPS.

Acknowledgements

The research was carried out within the state assignment of the Ministry of Education and Science of Russia (theme “Spin” No. AAAA-A18-118020290104-2 and theme “Electron” No. AAAA-A18-118020190098-5). The reported study was funded by RFBR, project number 19-33-60031. We acknowledge Elettra Sincrotrone Trieste for providing access to its synchrotron radiation facilities. I.P. and F.B. acknowledge financial support from EUROFEL project (RoadMap Esfri). The authors are grateful to Selezneva N.V. for XRD measurements and discussion.

References

[1] J.A. Wilson, A.D. Yoffe, The transition metal dichalcogenides discussion and interpretation of the observed optical, electrical and structural properties, Adv. Phys. 18 (1969) 193–335. https://doi.org/10.1080/00018736900101307.

[2] H. Cercellier, C. Monney, F. Clerc, C. Battaglia, L. Despont, M.G. Garnier, H. Beck, P. Aebi, L. Patthey, H. Berger, L. Forró, Evidence for an excitonic insulator phase in 1T-$TiSe_2$, Phys. Rev. Lett. 99 (2007) 146403. https://doi.org/10.1103/PhysRevLett.99.146403.

[3] C.M. Fang, R.A. de Groot, C. Haas, Bulk and surface electronic structure of 1T−TiS_2 and 1T-$TiSe_2$, Phys. Rev. B. 56 (1997) 4455–4463. https://doi.org/10.1103/PhysRevB.56.4455.

[4] B. Radisavljevic, A. Radenovic, J. Brivio, V. Giacometti, A. Kis, Single-layer MoS_2 transistors, Nat. Nanotechnol. 6 (2011) 147–150. https://doi.org/10.1038/nnano.2010.279.

[5] M.M. Ugeda, A.J. Bradley, Y. Zhang, S. Onishi, Y. Chen, W. Ruan, C. Ojeda-Aristizabal, H. Ryu, M.T. Edmonds, H.-Z. Tsai, A. Riss, S.-K. Mo, D. Lee, A. Zettl, Z. Hussain, Z.-X. Shen, M.F. Crommie, Characterization of collective ground states in single-layer $NbSe_2$, Nat. Phys. 12 (2016) 92–97. https://doi.org/10.1038/nphys3527.

[6] K. Rossnagel, L. Kipp, M. Skibowski, Charge-density-wave phase transition in 1T−$TiSe_2$: Excitonic insulator versus band-type Jahn-Teller mechanism, Phys. Rev. B. 65 (2002) 235101. https://doi.org/10.1103/PhysRevB.65.235101.

[7] R. Claessen, R.O. Anderson, J.W. Allen, C.G. Olson, C. Janowitz, W.P. Ellis, S. Harm, M. Kalning, R. Manzke, M. Skibowski, Fermi-liquid line shapes measured by angle-resolved photoemission spectroscopy on 1-T-$TiTe_2$, Phys. Rev. Lett. 69 (1992) 808–811. https://doi.org/10.1103/PhysRevLett.69.808.

[8] D. Gao, Q. Xue, X. Mao, W. Wang, Q. Xu, D. Xue, Ferromagnetism in ultrathin VS_2 nanosheets, J. Mater. Chem. C. 1 (2013) 5909. https://doi.org/10.1039/c3tc31233j.

[9] O. Lopez-Sanchez, D. Lembke, M. Kayci, A. Radenovic, A. Kis, Ultrasensitive photodetectors based on monolayer MoS_2, Nat. Nanotechnol. 8 (2013) 497–501. https://doi.org/10.1038/nnano.2013.100.

[10] M. Pumera, Z. Sofer, A. Ambrosi, Layered transition metal dichalcogenides for electrochemical energy generation and storage, J. Mater. Chem. A. 2 (2014) 8981–8987. https://doi.org/10.1039/C4TA00652F.

[11] K. Zhang, X. Fang, Y. Wang, Y. Wan, Q. Song, W. Zhai, Y. Li, G. Ran, Y. Ye, L. Dai, Ultrasensitive Near-Infrared Photodetectors Based on a Graphene–$MoTe_2$–Graphene Vertical van der Waals Heterostructure, ACS Appl. Mater. Interfaces. 9 (2017) 5392–5398. https://doi.org/10.1021/acsami.6b14483.

[12] E.A. Suslov, O. V. Bushkova, E.A. Sherstobitova, O.G. Reznitskikh, A.N. Titov, Lithium

intercalation into TiS_2 cathode material: phase equilibria in a Li–TiS_2 system, Ionics (Kiel). 22 (2016) 503–514. https://doi.org/10.1007/s11581-015-1566-0.

[13] B.P. Clayman, R.F. Frindt, The superconducting energy gap of $NbSe_2$, Solid State Commun. 9 (1971) 1881–1884. https://doi.org/10.1016/0038-1098(71)90574-6.

[14] M. Yoshida, J. Ye, T. Nishizaki, N. Kobayashi, Y. Iwasa, Electrostatic and electrochemical tuning of superconductivity in two-dimensional $NbSe_2$ crystals, Appl. Phys. Lett. 108 (2016) 202602. https://doi.org/10.1063/1.4950804.

[15] X. Xi, L. Zhao, Z. Wang, H. Berger, L. Forró, J. Shan, K.F. Mak, Strongly enhanced charge-density-wave order in monolayer $NbSe_2$, Nat. Nanotechnol. 10 (2015) 765–769. https://doi.org/10.1038/nnano.2015.143.

[16] J.Á. Silva-Guillén, P. Ordejón, F. Guinea, E. Canadell, Electronic structure of 2H-$NbSe_2$ single-layers in the CDW state, 2D Mater. 3 (2016) 035028. https://doi.org/10.1088/2053-1583/3/3/035028.

[17] C. Peng, H. Lyu, L. Wu, T. Xiong, F. Xiong, Z. Liu, Q. An, L. Mai, Lithium- and Magnesium-Storage Mechanisms of Novel Hexagonal $NbSe_2$, ACS Appl. Mater. Interfaces. 10 (2018) 36988–36995. https://doi.org/10.1021/acsami.8b12662.

[18] J. Zhang, C. Du, Z. Dai, W. Chen, Y. Zheng, B. Li, Y. Zong, X. Wang, J. Zhu, Q. Yan, NbS2 Nanosheets with M/Se (M = Fe, Co, Ni) Codopants for Li^+ and Na^+ Storage, ACS Nano. 11 (2017) 10599–10607. https://doi.org/10.1021/acsnano.7b06133.

[19] V. MAKARA, Hydrogen intercalates of low-dimensional dichalcogenides of transition metals, Int. J. Hydrogen Energy. 22 (1997) 233–239. https://doi.org/10.1016/S0360-3199(96)00159-0.

[20] L.M. Kulikov, A.A. Semjonov-Kobzar, M.M. Antonova, A.A. Chechovsky, L.G. Akselrud, R.V. Skolozdra, D. Fruchart, J.L. Soubeyroux, X-ray and neutron diffraction studies of the formation and structure of hydrogen intercalated 2H-$NbSe_2$ phases, J. Alloys Compd. 244 (1996) 11–15. https://doi.org/10.1016/S0925-8388(96)02427-9.

[21] M.A. Obolensky, A. V. Basteev, L.A. Bazyma, Hydrogen Storage in Irradiated Low-Dimensional Structures, Fullerenes, Nanotub. Carbon Nanostructures. 19 (2010) 133–136. https://doi.org/10.1080/1536383X.2010.490134.

[22] M.S. Whittingham, The electrochemical characteristics of VSe_2 in lithium cells, Mater. Res. Bull. 13 (1978) 959–965. https://doi.org/10.1016/0025-5408(78)90108-3.

[23] C. Yang, J. Feng, F. Lv, J. Zhou, C. Lin, K. Wang, Y. Zhang, Y. Yang, W. Wang, J. Li, S. Guo, Metallic Graphene-Like VSe_2 Ultrathin Nanosheets: Superior Potassium-Ion Storage and Their Working Mechanism, Adv. Mater. 30 (2018) 1800036. https://doi.org/10.1002/adma.201800036.

[24] C.F. van Bruggen, C. Haas, Magnetic susceptibility and electrical properties of VSe_2 single crystals, Solid State Commun. 20 (1976) 251–254. https://doi.org/10.1016/0038-1098(76)90187-3.

[25] D.J. Eaglesham, R.L. Withers, D.M. Bird, Charge-density-wave transitions in 1T-VSe_2, J. Phys. C Solid State Phys. 19 (1986) 359–367. https://doi.org/10.1088/0022-3719/19/3/006.

[26] J. Yang, W. Wang, Y. Liu, H. Du, W. Ning, G. Zheng, C. Jin, Y. Han, N. Wang, Z. Yang, M. Tian, Y. Zhang, Thickness dependence of the charge-density-wave transition temperature in VSe_2, Appl. Phys. Lett. 105 (2014) 063109. https://doi.org/10.1063/1.4893027.

[27] M. Obolensky, K. Chashka, V. Beletsky, A. Basteev, V. Solovey, Hydrogen in layer structures, Int. J. Hydrogen Energy. 18 (1993) 217–222. https://doi.org/10.1016/0360-3199(93)90022-3.

[28] M.S. Brezhestovskii, E.A. Suslov, O. V. Bushkova, A.I. Merentsov, A.N. Titov, Influence of heterovalent substitution in the titanium sublattice on the electrochemical intercalation of lithium in $M_yTi_{1-y}Se_2$ (M = Cr, V)), Phys. Solid State. 57 (2015) 2078–2086. https://doi.org/10.1134/S106378341510008X.

[29] I.S. Kwon, I.H. Kwak, J.Y. Kim, T.T. Debela, Y.C. Park, J. Park, H.S. Kang, Concurrent Vacancy and Adatom Defects of $Mo_{1-x}Nb_xSe_2$ Alloy Nanosheets Enhance Electrochemical Performance of Hydrogen Evolution Reaction, ACS Nano. 15 (2021) 5467–5477. https://doi.org/10.1021/acsnano.1c00171.

[30] M. Bayard, B.F. Mentzen, M.J. Sienko, Synthesis and structural aspects of the vanadium-substituted niobium diselenides, Inorg. Chem. 15 (1976) 1763–1767. https://doi.org/10.1021/ic50162a005.

[31] I. Naik, G.C. Tiwari, C.S. Yadav, A.K. Rastogi, Effect of magnetic exchange interaction in resistivity on 2H-$Nb_{1-x}V_xSe_2$, Indian J. Phys. 87 (2013) 1075–1078. https://doi.org/10.1007/s12648-013-0331-3.

[32] M. Zangrando, M. Finazzi, G. Paolucci, G. Comelli, B. Diviacco, R.P. Walker, D. Cocco, F. Parmigiani, BACH, the beamline for advanced dichroic and scattering experiments at ELETTRA, Rev. Sci. Instrum. 72 (2001) 1313. https://doi.org/10.1063/1.1334626.

[33] J. Libra, KolXPD: Spectroscopy Data Measurement and Processing, KolXPD. (2017). https://www.kolibrik.net/en/kolxpd.

[34] A.S. Shkvarin, Y.M. Yarmoshenko, M.V. Yablonskikh, A.I. Merentsov, E.G. Shkvarina, A.A. Titov, Y.M. Zhukov, A.N. Titov, The electronic structure formation of Cu_xTiSe_2 in a wide range ($0.04 < x < 0.8$) of copper concentration, J. Chem. Phys. 144 (2016) 074702. https://doi.org/10.1063/1.4941767.

[35] A.S. Shkvarin, Y.M. Yarmoshenko, A.I. Merentsov, I. Píš, F. Bondino, E.G. Shkvarina, A.N. Titov, Guest–Host Chemical Bonding and Possibility of Ordering of Intercalated Metals in Transition-Metal Dichalcogenides, Inorg. Chem. 57 (2018) 5544–5553. https://doi.org/10.1021/acs.inorgchem.8b00511.

[36] F. Göhler, G. Mitchson, M.B. Alemayehu, F. Speck, M. Wanke, D.C. Johnson, T. Seyller, Charge transfer in $(PbSe)_{1+\delta}(NbSe_2)_2$ and $(SnSe)_{1+\delta}(NbSe_2)_2$ ferecrystals investigated by photoelectron spectroscopy, J. Phys. Condens. Matter. 30 (2018) 055001.

https://doi.org/10.1088/1361-648X/aaa212.

[37] S.A. Howard, C.N. Singh, G.J. Paez, M.J. Wahila, L.W. Wangoh, S. Sallis, K. Tirpak, Y. Liang, D. Prendergast, M. Zuba, J. Rana, A. Weidenbach, T.M. McCrone, W. Yang, T.-L. Lee, F. Rodolakis, W. Doolittle, W.-C. Lee, L.F.J. Piper, Direct observation of delithiation as the origin of analog memristance in Li_xNbO_2, APL Mater. 7 (2019) 071103. https://doi.org/10.1063/1.5108525.

[38] A. O'Hara, T.N. Nunley, A.B. Posadas, S. Zollner, A.A. Demkov, Electronic and optical properties of NbO_2, J. Appl. Phys. 116 (2014) 213705. https://doi.org/10.1063/1.4903067.

[39] R.Z. Bachrach, Synchrotron Radiation Research Advances in Surface and Interface Science, Springer US, Boston, MA, 1992. https://doi.org/10.1007/978-1-4615-3278-1.

[40] A. Kay, Multi-Atom Resonant Photoemission: A Method for Determining Near-Neighbor Atomic Identities and Bonding, Science (80-.). 281 (1998) 679–683. https://doi.org/10.1126/science.281.5377.679.

[41] J.-E. Rubensson, J. Lüning, S. Eisebitt, W. Eberhardt, It's always a one-step process, Appl. Phys. A Mater. Sci. Process. 65 (1997) 91–96. https://doi.org/10.1007/s003390050549.

[42] N. Mårtensson, M. Weinelt, O. Karis, M. Magnuson, N. Wassdahl, A. Nilsson, J. Stöhr, M. Samant, Coherent and incoherent processes in resonant photoemission, Appl. Phys. A Mater. Sci. Process. 65 (1997) 159–167. https://doi.org/10.1007/s003390050559.

[43] S. Hüfner, S.-H. Yang, B.S. Mun, C.S. Fadley, J. Schäfer, E. Rotenberg, S.D. Kevan, Observation of the two-hole satellite in Cr and Fe metal by resonant photoemission at the 2p absorption energy, Phys. Rev. B. 61 (2000) 12582–12585. https://doi.org/10.1103/PhysRevB.61.12582.

[44] A.S. Shkvarin, Y.M. Yarmoshenko, A.I. Merentsov, E.G. Shkvarina, A.F. Gubkin, I. Píš, S. Nappini, F. Bondino, I.A. Bobrikov, A.N. Titov, Electronic Structures of the Vanadium-Intercalated and Substitutionally Doped Transition-Metal Dichalcogenides

$Ti_xV_ySe_2$, Inorg. Chem. 59 (2020) 8543–8551. https://doi.org/10.1021/acs.inorgchem.0c00953.

[45] A.I. Merentsov, A.S. Shkvarin, M.S. Postnikov, L. Gregoratti, M. Amati, P. Zeller, P. Moras, A.N. Titov, Studying the heterogeneity of the $Cr_xTi_{1-x}Ch_2$ (Ch = S, Se) single crystals using X-ray scanning photoemission microscopy, J. Phys. Chem. Solids. 160 (2022) 110309. https://doi.org/10.1016/j.jpcs.2021.110309.

[46] C. Gong, H. Zhang, W. Wang, L. Colombo, R.M. Wallace, K. Cho, Band alignment of two-dimensional transition metal dichalcogenides: Application in tunnel field effect transistors, Appl. Phys. Lett. 103 (2013) 053513. https://doi.org/10.1063/1.4817409.

[47] V. Grasso, ed., Electronic Structure and Electronic Transitions in Layered Materials, Springer Netherlands, Dordrecht, 1986. https://doi.org/10.1007/978-94-009-4542-5.

[48] A.R. Beal, H.P. Hughes, W.Y. Liang, The reflectivity spectra of some group VA transition metal dichalcogenides, J. Phys. C Solid State Phys. 8 (1975) 4236–4234. https://doi.org/10.1088/0022-3719/8/24/015.

Supporting information

Peculiarities of the electronic structure of structural fragments in $Nb_{1-x}V_xSe_2$ materials: synchrotron radiation spectroscopy study

A.I. Merentsov[1], A.S. Shkvarin[1], E.M. Sherokalova[2], I. Píš[3,4], F. Bondino[4], A.N. Titov[1]

[1] M.N. Miheev Institute of Metal Physics of Ural Branch of Russian Academy of Sciences, 620990 Ekaterinburg, Russia

[2] Ural Federal University, 620002 Ekaterinburg, Russia

[3] Elettra-Sincrotrone Trieste S.C.p.A, S.S. 14 – km 163.5, 34149 Basovizza, Trieste, Italy

[4] IOM-CNR, Laboratorio TASC, S.S. 14 – km 163.5, 34149 Basovizza, Trieste, Italy

X-ray diffraction study of the $Nb_{1-x}V_xSe_2$ single crystals (Figure S1) and powders (Figure S2) was performed using a Bruker AXS D8 Advance diffractometer (room temperature, Cu $K\alpha_{1,2}$ radiation, Göbel mirror monochromator, and a set of Soller slits for limiting the axial divergence of the diffracted beam). The data for the powder samples are in good agreement with those reported in Ref. [1] confirming the mixture of 2H and 4Hb phases with prevailing 4Hb phase.

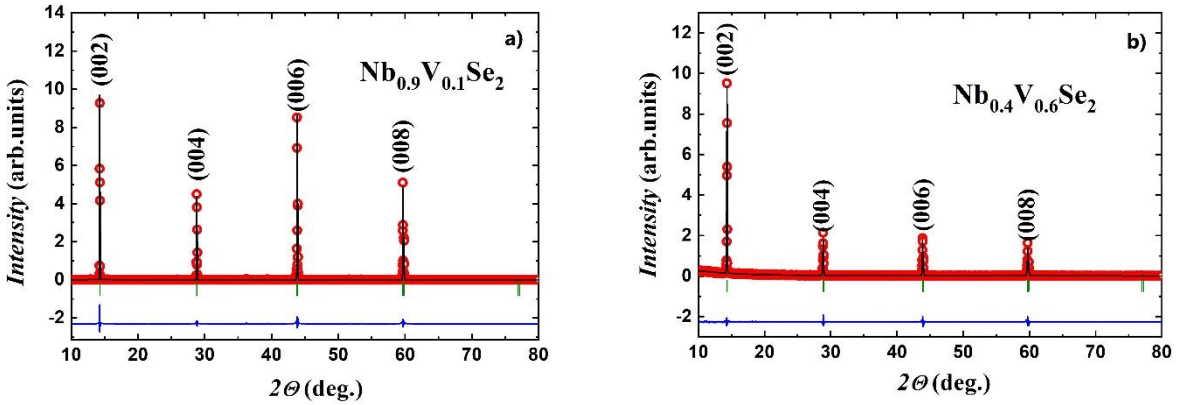

Figure S1. X-ray diffraction patterns for $Nb_{0.9}V_{0.1}Se_2$ (a) and $Nb_{0.4}V_{0.6}Se_2$ (b) single crystals. Red circles - observed profile, black line - calculated profile, blue line - difference curve (I_{obs} - I_{calc}).

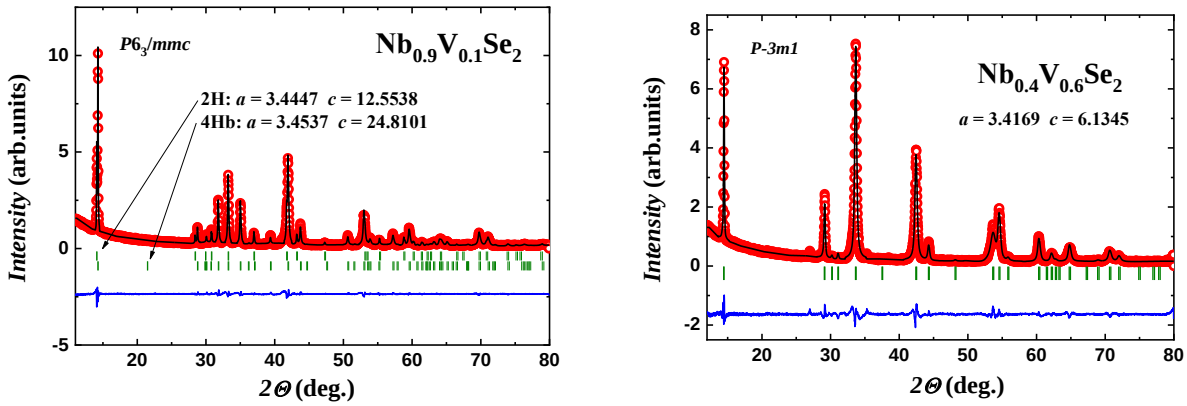

Figure S2. X-ray diffraction patterns for $Nb_{0.9}V_{0.1}Se_2$ (a) and $Nb_{0.4}V_{0.6}Se_2$ (b) powders. Red circles - observed profile, black line - calculated profile, blue line - difference curve (I_{obs} - I_{calc}). The *a* and *c* lattice parameters slightly differ from those calculated from the single-crystal XRD data, however, remain in good agreement with those obtained in Ref. [1].

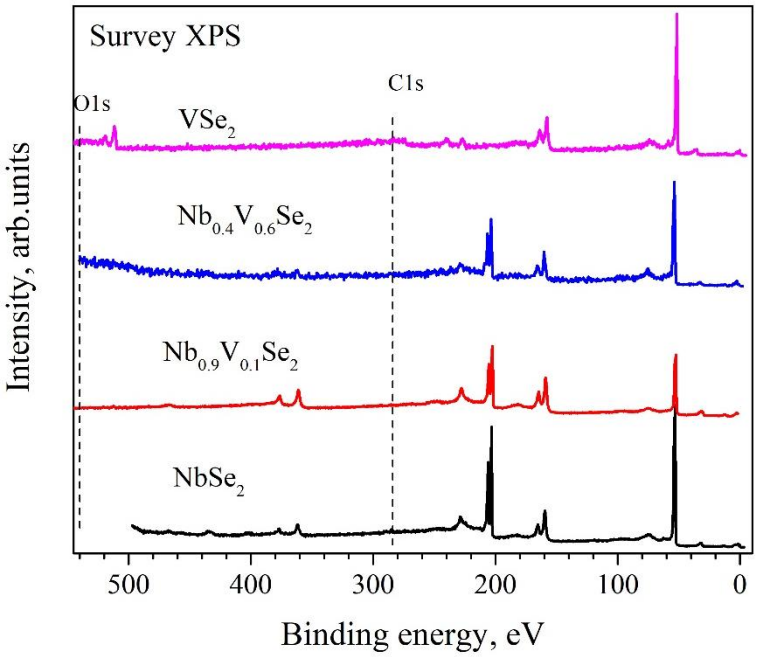

Figure S3. Survey spectra for $Nb_{1-x}V_xSe_2$ single crystals. Dashed vertical lines mark the C 1s and O 1s binding energies. The absence of the C 1s and O 1s peaks in the survey spectra for all the studied crystals indicates a good quality of the surfaces.

Figure S4 (a) shows the V $L_{2,3}$ XAS spectra. The structure of all the spectra is typical for V $L_{2,3}$ and contains a prepeak A and peaks B (corresponding to e_g states) and C (corresponding to t_{2g} states) [2]. The shape of the spectra substantially depends on V concentration: the B peak clearly visible for VSe_2 is almost invisible in the spectrum for $Nb_{0.4}V_{0.6}Se_2$. The Nb $M_{2,3}$ XAS spectra (Figure S4 (b)) are also V concentration dependent. The increase in the Nb by V substitution results in the broadening and a slight shift of the main peak ($h\nu$ = 364 eV).

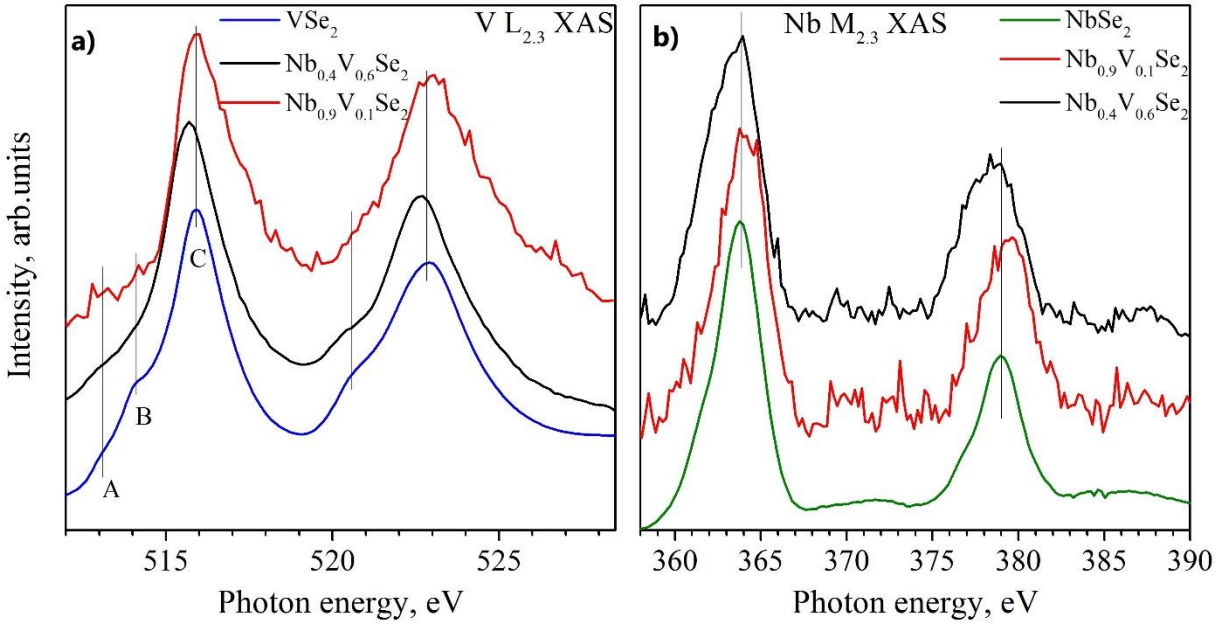

Figure S4. V $L_{2,3}$ XAS (a) and Nb $M_{2,3}$ XAS (b) for $Nb_{1-x}V_xSe_2$.

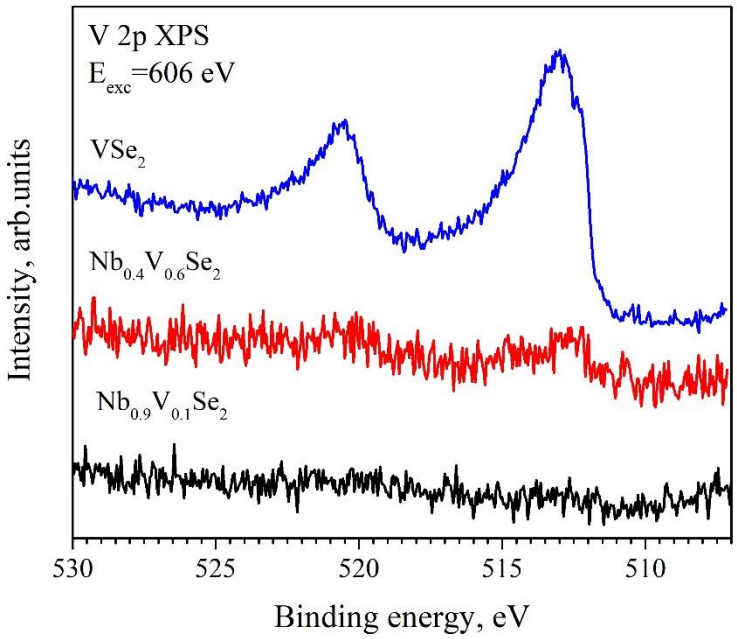

Figure S5. The V 2p core-level spectra for $Nb_{1-x}V_xSe_2$. The low intensity of the spectra for $Nb_{0.4}V_{0.6}Se_2$ and $Nb_{0.9}V_{0.1}Se_2$ does to allow to make a conclusion about their exact binding energy positions.

[1] M. Bayard, B.F. Mentzen, M.J. Sienko, Synthesis and structural aspects of the vanadium-substituted niobium diselenides, Inorg. Chem. 15 (1976) 1763–1767. https://doi.org/10.1021/ic50162a005.

[2] M.G. Brik, K. Ogasawara, H. Ikeno, I. Tanaka, Fully relativistic calculations of the L2,3-edge XANES spectra for vanadium oxides, Eur. Phys. J. B. 51 (2006) 345–355. https://doi.org/10.1140/epjb/e2006-00243-5.